ELSEVIER

S0032-3861(96)00591-5

Polymer Vol. 38 No. 4, pp. 887–895, 1997

0032-3861/97/$17.00 + 0.00

Dielectric study of a ferroelectric side-chain liquid crystalline polysiloxane with a broad temperature range of the chiral smectic C phase: 2. Doping effect of a non-linear optically active dye

Ging-Ho Hsiue* and Rong-Ho Lee
Department of Chemical Engineering, National Tsing Hua University, Hsinchu, Taiwan 300, ROC

and Ru-Jong Jeng
Department of Chemical Engineering, National Chung Hsing University, Taichung, Taiwan 400, ROC
(Received 15 December 1995; revised 25 April 1996)

Dielectric relaxation behaviour of the guest–host mixture of a ferroelectric side chain liquid crystalline polymer (FLCP) and a nonlinear optical (NLO) dye has been investigated with broadband dielectric relaxation spectroscopy. The liquid crystal (LC) phases of these guest–host materials were characterized with the differential scanning calorimeter, optical polarizing microscopy, and X-ray diffractometer. No phase separation is observed when the doping level of the NLO dye is below 10 wt%. The doping of the NLO dye into the FLCP results in the significant increase of the relaxation intensity and frequency of the Goldstone mode in the chiral smectic C phase (S_C*). Moreover, the NLO dye has high relaxation intensity in the LC phase for such guest–host material. On the other hand, the occurrence of phase separation is observed when the doping level of the NLO dye is 30% by weight. The phase separation results in the reduction of the relaxation intensity for both the Goldstone mode of the FLCP and molecular motion of the NLO dye. The relationship between the thermal dynamic behaviour and the environment around molecules for such NLO active guest–host material was discussed in great detail.

(Keywords: ferroelectric liquid crystalline polymers; molecular relaxation; collective relaxation)

INTRODUCTION

Ferroelectric liquid crystals (FLCs) with large spontaneous polarization in the chiral smectic C (S_C*) phase have potential for applications in the fast response display, light valve memory devices[1,2]. FLC has one or two chiral carbons in their molecular structure in which a centre of inversion symmetry is absent. Therefore, FLC can be second-order nonlinear optically active[3,4]. The second-order nonlinear optical (NLO) properties of FLC have recently attracted much attention[5,6]. However, the second harmonic generation (SHG) signal of the FLC was weaker compared to the NLO-active amorphous polymer. In order to resolve this problem, a new concept that an NLO dye was doped into the FLC to enhance the SHG was reported[7]. In such FLC/NLO dye guest–host system, low viscosity of the FLC results in a weak surface stabilized effect, when compared to the FLCP in a thin cell[8]. The excellent surface stabilized characteristic of the FLCP would be helpful for the alignment of the mesogenic group after the removal of the electric poling field. Consequently, the FLCP/NLO dye system will exhibit a better thermal stability of SHG than the FLC/NLO dye system.

NLO properties are proportional to both chromophore density and electric poling efficiency of the NLO dye and mesogenic group of FLCP in such FLCP/NLO dye guest–host materials. Moreover, the poling efficiency is closely associated with the ease of reorientation of the mesogenic group and NLO dye under an applied electric field. When a FLCP exhibits high molecular mobility in the fluctuation of the director of the tilt angle (Goldstone mode), the threshold field for switching can be lowered. As a result of that, the helical structure of the FLCP in the S_C* phase can be unwound completely, and the SHG efficiencies will be enhanced[8]. Moreover, the mobility of the mesogenic group is dependent on the chemical structure and environment around the molecular FLCP. The doping of the low molecular weight NLO dye into the S_C* phase would enhance the thickness of the smectic layer[9], and results in the high molecular mobility of the mesogenic group for FLCP. This will better the alignment of the mesogenic group during the

* To whom correspondence should be addressed. Also at Department of Chemical Engineering, National Chung Hsing University, Taichung, Taiwan 400, ROC

electric poling process. In addition, the self-alignment characteristic of the liquid crystal phase is helpful for the alignment of the NLO dyes for such guest–host material under an applied electric poling field. Therefore, the poling efficiency (i.e. SHG intensity) of this guest–host material are related to the thermal behaviour of the FLCP and NLO dye. The study of the thermal dynamics behaviour of the NLO dye in FLCP, therefore, becomes a pertinent topic. Dielectric relaxation measurement is a useful technique for studying the thermal dynamic behaviour of the FLCP, since it measures the molecular motions of the dipole moments of the mesogenic groups directly.

In this paper, a FLCP has been used as a polymer matrix. This FLCP possesses a wide temperature range of liquid crystalline (LC) phase from room temperature to 230°C[10]. The wide temperature range of the LC phase will not disappear even though a large quantity (30%) of NLO dye is doped into FLCP. A NLO dye (disperse orange 3, DO3) with a large second-order susceptibility is chosen as the guest molecule. The doping effect of the NLO dye on the dielectric relaxation behaviour of the FLCP is studied. Moreover, the molecular mobility of the NLO dye in such guest–host material are also reported.

EXPERIMENTAL

In this study, the NLO active dye. DO3 (*Figure 1A*); Aldrich Chemical, Co.) was used as the guest molecules to be doped into the host of FLCP (*Figure 1B*). The details of the synthesis and characterizations of the FLCP have been reported by Hsu *et al.*[10]. The mixtures of FLCP and DO3 (FLCP/DO3) with different weight fraction ratios (sample I: 95/5, sample II: 90/10, and sample III: 70/30) were obtained by dissolving the compounds in chloroform. The solution of the mixtures was left in the hood for 8 h and then kept in vacuum oven at room temperature for another 8 h to completely dry

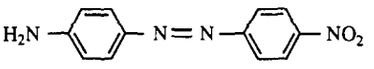

K 212°C I

(a) DO3

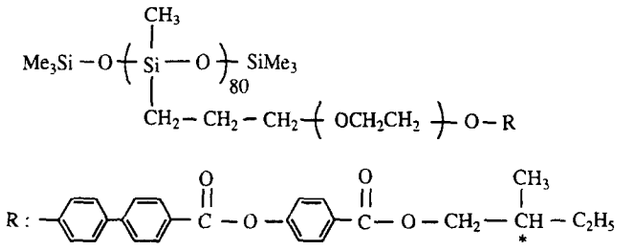

Heating (°C): G 9.8 S_C* 215.2 S_A 234.6 I

Cooling (°C): I229.2 S_A 211.7 S_C* 4.1 G

(b) FLCP

Figure 1 Chemical structures of (a) DO3 and (b) FLCP, respectively

out chloroform. The thermal transitions of FLCP/DO3 were determined by Differential Scanning Calorimeter (Seiko SSC/5200 DSC). The thermal transitions were read at the maximum of their endothermic or exothermic peaks. Glass transition temperature was read at the middle of the change in heat capacity. Heating and cooling rates were 10°C min^{-1} in all of these cases. The transitions were collected from the second heating and cooling scans. A Nikon Microphot-FX optical polarized microscope equipped with a Mettler FP82 hot stage and a Mettler FP80 central processor was applied toward observing anisotropic textures. X-ray diffraction measurement was performed using a nickel-filtered CuK_α radiation (Rigaku Powder Diffractometer). The dielectric spectroscopy was determined on a Novercontrol GmbH. Measurements were performed by a Schlumberger SI 1260 impedance/gain-phase analyser (frequency: 10^{-1}–10^6 Hz) and a Quator temperature controller. The measurement system is fully computer controlled. A nitrogen gas heating system ranged from 100 K to 550 K was used. The temperature was adjusted within the tolerance of ±0.1 K. The FLCP samples were sandwiched between two parallel metal electrode plates with a spacer of 50 μm.

RESULTS AND DISCUSSION

The d.s.c. heating and cooling traces of FLCP/DO3 with different weight fraction ratios (samples I, II, III) are shown in *Figure 2*. The thermal transition temperatures and their corresponding enthalpy changes of these three samples are summarized in *Table 1*. Samples I and II exhibited enantiotropic smectic A (S_A) and chiral smectic C (S_C*) phases. The phase separation was not observed for these two samples (curves A, B, C and D), whereas

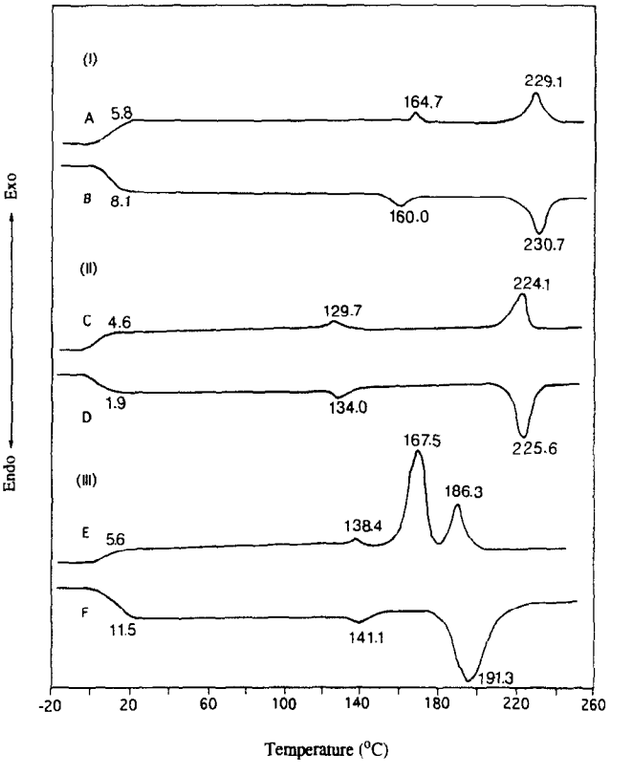

Figure 2 D.s.c. thermograms of the samples I–III (curves A, C, E: cooling scan; curves B, D, F: heating scan)

Table 1 Phase transitions and phase transition enthalpies for the samples I–III

Sample		Phase transitions[a], °C (corresponding enthalpy changes, kJ kg^{-1})
I	heating	G 8.1 S_C* 160.0 (0.6) S_A 230.7 (5.9) I
	cooling	I 229.1 (4.1) S_A 164.7 (0.3) S_C* 5.8 G
II	heating	G 1.9 S_C* 134.0 (0.4) S_A 225.6 (8.1) I
	cooling	I 224.1 (5.5) S_A 129.7 (0.3) S_C* 4.6 G
III	heating	G 11.5 S_C* 141.1 (0.5) S_A 191.3[b] (27.8) I
	cooling	I 186.3 (5.1) S_A 167.5[b] (17.0) S_A 138.4 (0.4) S_C* 5.6 G

[a] G: glass transition, S_A: smectic A phase, S_C*: chiral smectic C phase, I: isotropic phase
[b] The melting point of the crystallite in the LC phase

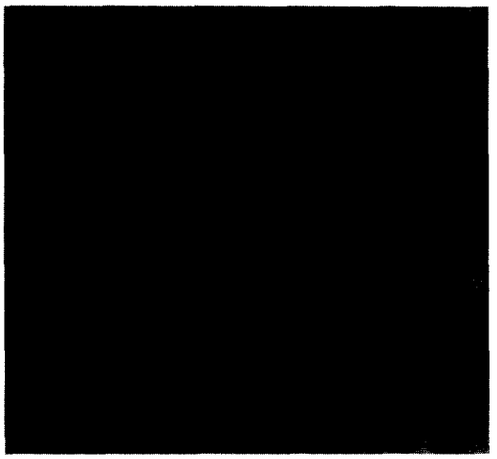

(a)

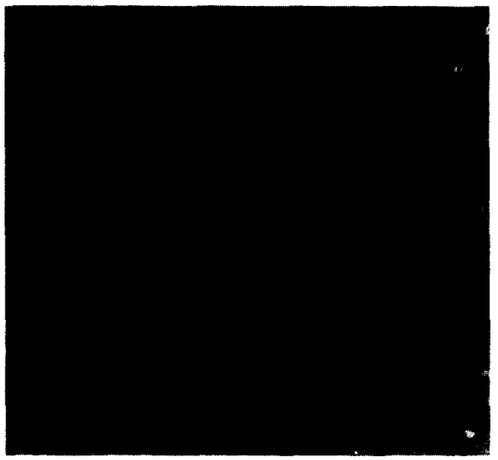

(b)

Figure 3 Optical polarizing micrographs of the samples II and III ((a) S_C* texture obtained after cooling to 110°C for sample II, 800×; (b) S_C* texture obtained after cooling to 125°C for sample III, 800×)

the phase separation was observed (curves E and F) for sample III. Aggregation of DO3 molecules formed an additional melting transition at 191.3°C on the heating scan and a crystallization transition at 167.5°C on the cooling scan for sample III. The transition enthalpy of the melting point was higher than other transitions. Moreover, the transition temperature and enthalpy change of this crystallite was not the same as that of the pure DO3 sample. The transition temperature and enthalpy change of the pure DO3 sample were 212.0°C and 84.6 kJ kg^{-1}, respectively. For sample III, the LC domain revealed a S_C* to S_A phase transition at 141.1°C on the d.s.c. heating scan (curve F). Its S_A to isotropic phase transition was overlapped with the melting transition of the crystallite. On the cooling scan (curve E), the isotropic phase to S_A phase transition and S_A to S_C* phase transition were present at 186.3°C and 138.4°C, respectively. Moreover, the phase transition temperatures decreased with the increasing content of the NLO dye for samples I, II and III. The doping of the NLO dye into FLCP seems to reduce the thermal stability of LC phases. In addition, the texture of the mesophase for these samples (I, II, and III) was observed by POM. The S_A and S_C* phases were observed when the temperature was cooling from the isotropic phase for these three samples. The cooling rate was 0.1°C min^{-1}. The fan-shaped focal-comic texture of the S_C* phase for samples II and III are shown in *Figures 3a* and *b*, respectively.

The X-ray diffraction diagrams obtained from the powder samples of II and III at different temperatures are shown in *Figures 4a* and *b*, respectively. In *Figure 4a*, a broad reflection at wide angle and a sharp reflection at low angle were assigned to be the lateral packing and the smectic layer, respectively. In the S_A phase, the thickness of smectic layer was not varied with increasing temperature above 140°C. The thickness of the smectic layer decreased with decreasing temperature corresponding to the increase of the tilt angle in the S_C* phase. The X-ray diffraction result indicated that no phase separation occurred for sample II. The X-ray diffraction diagram of sample I is similar to that of sample II. For sample III, several sharp reflections as well as a broad reflection were observed at wide angle region (*Figure 4b*). This reflects the existence of the DO3 crystallites and the LC domain individually. The decrease of the broad and sharp reflection angles (2θ) with increasing temperature implied the variation of the thickness of the smectic layer in the LC phases. The LC phases did not disappear even though the phase separation occurred. The thickness of the smectic layer *versus* temperature for samples I, II and III are shown in *Figure 5*. The thickness of the smectic layer increased with the increasing content of DO3 because of the uniform distribution of DO3 between the side chain groups. When an excessive amount of DO3 was further added, the thickness of the smectic layer was not further enhanced. This is due to the occurrence of the phase separation. The excessive amount of DO3 was not dissolved into the LC phase,

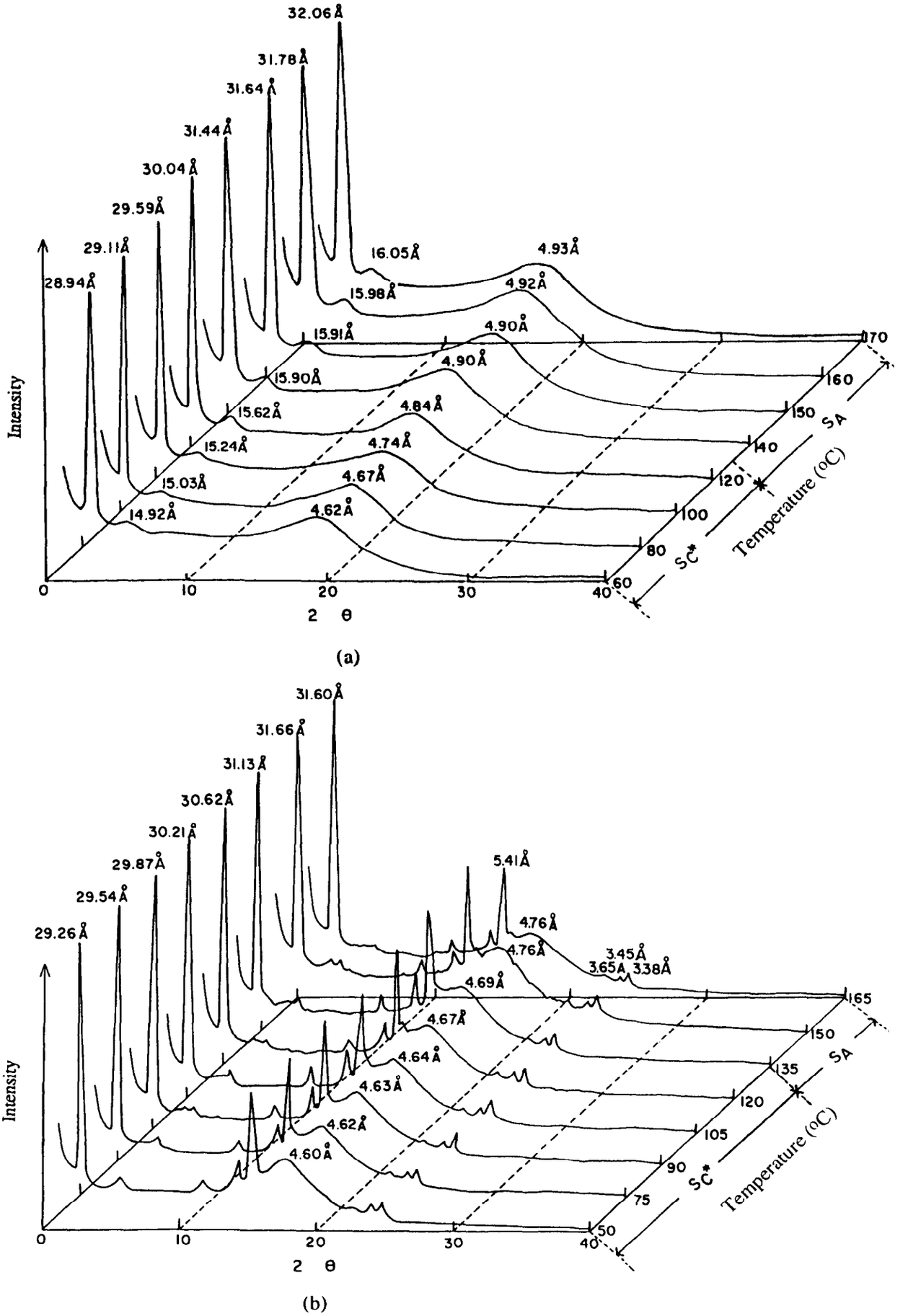

Figure 4 Temperature dependent X-ray diffraction diagrams for samples (a) II and (b) III, respectively

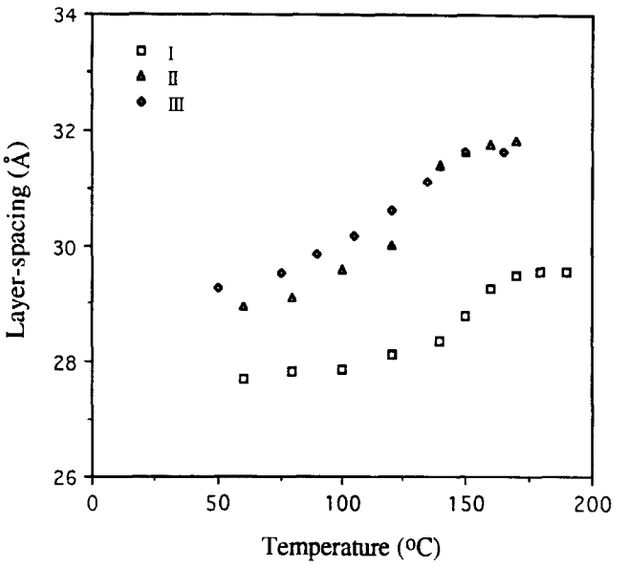

Figure 5 The layer spacing as a function of temperature in the liquid crystal phases of samples I–III

but formed the crystallite. Furthermore, the thickness of the smectic layer decreased remarkably with decreasing temperature due to the increases of the tilt angle at the transition temperature of S_A and S_C* phases. The thickness of the smectic layer remained almost constant as the temperature further decreased owing to the gradual decrease of the variation of the tilt angle.

The dielectric constant *versus* temperature and frequency for samples FLCP, I and III are shown in *Figures 6a–c*, respectively. For sample FLCP, the dielectric constant increase with increasing temperature in the S_C* phase. The dielectric constant increased remarkably in the neighbourhood of the S_A–S_C* transition temperature because of the presence of the Goldstone and Soft modes. These two ferroelectric modes have been observed in several FLCPs by Vallerien *et al.*[11–16]. The Goldstone mode shows up in the S_C* phase resulting from the fluctuation of the director of the tilt vector at constant tilt angle. The Soft mode corresponding to the fluctuation of the tilt angle (between the molecular director and the normal to the smectic layers) appears in the neighbourhood of the S_A–S_C* transition temperature. Moreover, the major contribution to the increase of the dielectric constant was the Goldstone mode due to the large fluctuation of the spontaneous polarization vector[11–16]. However, the relaxation peak (maximum value of the dielectric constant) of the Goldstone mode was not observed in the S_C* phase for sample FLCP due to the relaxation frequency being below 1 Hz[17]. In contrast, the large amplitude of the Goldstone mode was observed in the S_C* phase at a frequency between 1 Hz and 100 Hz for sample I. The doping of the low molecular weight NLO dye in the LC phase lead to the increase of the thickness of the smectic layer in the S_C* phase for the FLCP. The loosening of a denser packing of the higher tilted smectic phase results in the relaxation frequency of the Goldstone mode shifting toward the higher frequency range. Moreover, the relaxation intensity of the Goldstone mode was also enhanced remarkably due to the existence of the NLO dye in FLCP. The increase of the relaxation intensity and frequency of the Goldstone mode was important for the electro-optical application of the FLCP. Kalmykov *et al.* have reported that the electro-optical switching time (τ) is related to the dielectric parameters of the Goldstone mode relaxation[18]

$$\tau = \frac{\tau_G P_S}{2\epsilon_O \Delta\epsilon_G E} \quad (1)$$

The switching time is dependent on the relaxation time (τ_G) and dielectric relaxation intensity ($\Delta\epsilon_G$) of the Goldstone mode. The doping of the NLO dye in the S_C* phase lead to the increase of the relaxation intensity and the reduction of the relaxation time of the Goldstone mode. As a result of that, the switching was facilitated. This is favourable for the alignment of the mesogenic groups of the FLCP during the electric poling process. For sample III, the amplitude of the Goldstone mode was smaller than sample I. The formation of the crystalline domain in the LC phase restricted the molecular mobility of the Goldstone mode as the phase separation occurred for sample III.

The dielectric loss tangent as a function of temperature and frequency for samples I and III are given in *Figures 7a* and *b*, respectively. The molecular (α-, β-, γ-relaxation) relaxations of the FLCP are clearly observed. The β- and γ-relations occurred below T_g. These two relaxations correspond to the reorientation of the mesogenic group and spacer group of the FLCP, respectively[19]. The broad relaxation temperature distribution of these two relaxations reflect local and noncooperative motions of side chain groups[20]. In addition, the α- and σ-relaxations have been observed at the higher temperature range. The α-relaxation was the process to be associated with the glass transition. In other words, the relaxation is attributed to a combination of motions of polymer main chain and side chain group. The σ-relaxation corresponds to the molecular motion of the DO3. For sample I, the α-relaxation was covered by the σ-relaxation at a frequency below 10^4 Hz due to the higher relaxation intensity of the σ-relaxation. The σ-relaxation temperature shifts toward the higher temperature range with increasing the measuring frequency. The relaxation behaviour of the α- and σ-relaxations for sample II was the same as that for sample I. For sample III, the α-relaxation was not covered by the σ-relaxation due to the decrease of the intensity of the σ-relaxation. The σ-relaxation intensity was reduced because of the occurrence of phase separation. The aggregation of the DO3 molecules lead to the decrease of the molecular mobility. Moreover, the α-relaxation coincided with the σ-relaxation at lower frequency range (10^3 Hz). Then, these two relaxations separated with the increasing measured frequency. Furthermore, the δ-relaxation was not observed above T_g, which corresponded to the rotation of side chain group around the polymer backbone. The δ-relaxation was not observed due to the overlap of the collective relaxations for these three samples. At the higher temperature range, the existence of the Goldstone and Soft models lead to remarkable increase of the dielectric loss in the S_C* phase. The amplitude of the Goldstone mode for sample I was larger than that of sample III. As the temperature further increased, the melting transition of the crystallite was observed for sample III. This transition was also observed at 191.3°C on the heating scan of d.s.c.

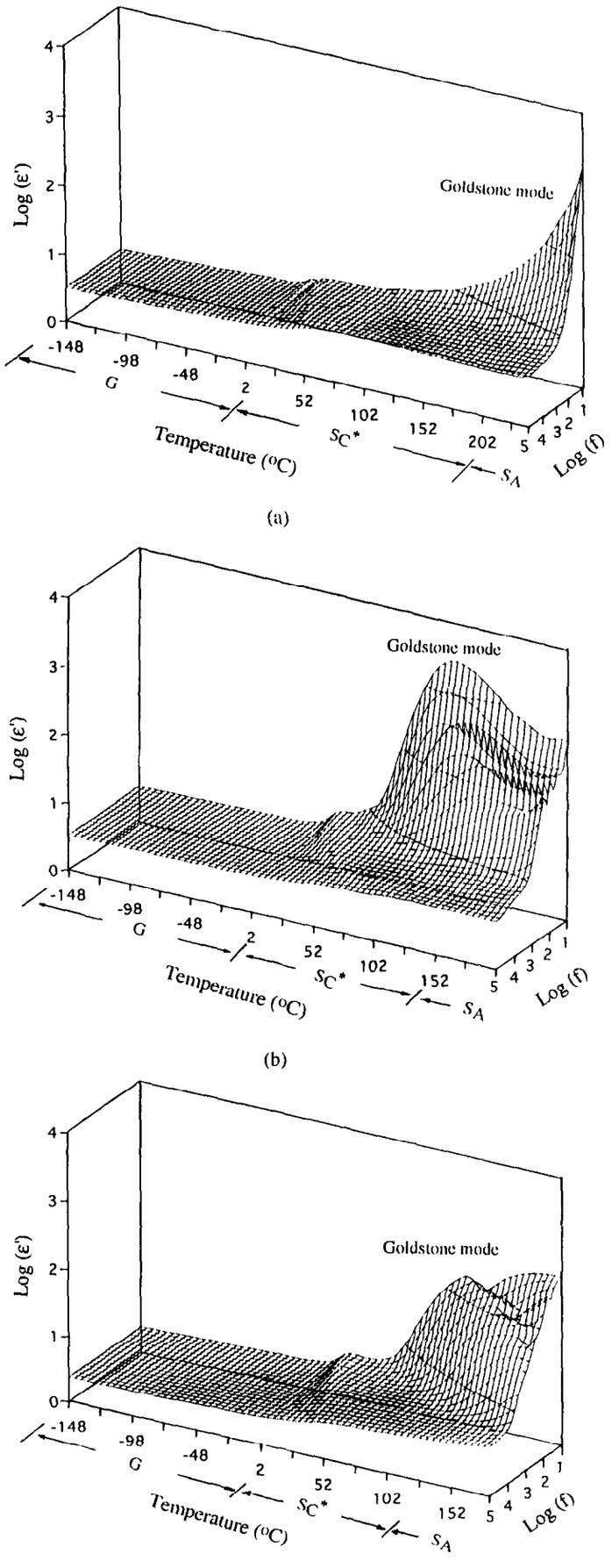

Figure 6 The dielectric constant as a function of temperature and logarithm of frequency for the samples (a) FLCP, (b) I, and (c) III, respectively

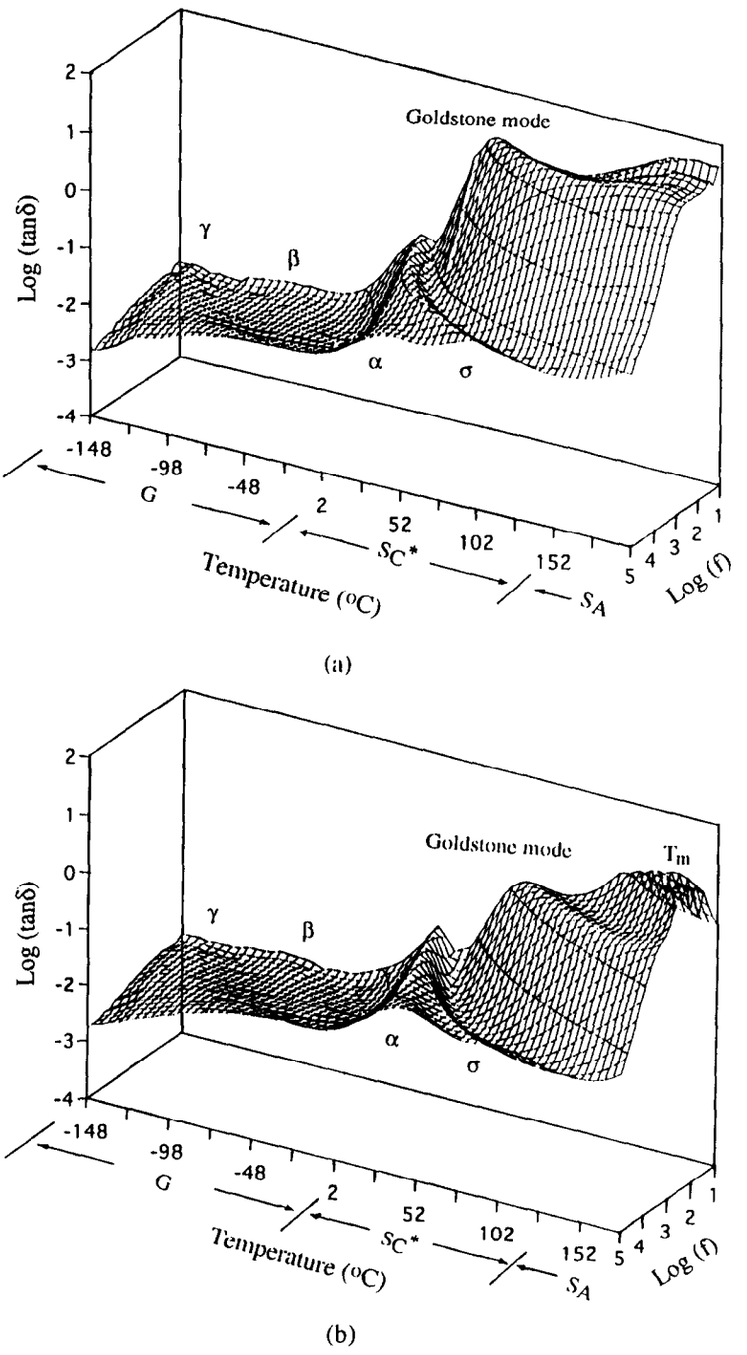

Figure 7 The dielectric loss tangent as a function of temperature and logarithm of frequency for the samples (a) I, and (b) III, respectively

When the relaxation frequencies are plotted as a function of the reciprocal of temperature (*Figure 8*), a straight line similar to the characteristic of an Arrhenius plot was obtained except for the α- and σ-relaxations of the samples. The non-linear character of the α- and σ-relaxations were obtained for these samples. The non-linear character indicates that the α-relaxation could be identified as the glass transition[21]. The activation energies of the dielectric relaxations are summarized in *Table 2*. FLCP exhibits a larger tilt angle at temperature near T_g in the S_C* phase. The tilt angle becomes smaller as the temperature increases. The rotational freedom of NLO dye was decreased in the tighter pitch (i.e., larger tilt angle) of the S_C* phase by steric hindrance near T_g[22]. As a result, the high activation energy of the σ-relaxation was obtained at a lower frequency range (below 10^4 Hz). The activation energy was decreased with the decreasing steric hindrance at a higher temperature range. The activation energy of the α-relaxation could not be obtained at lower frequency range for samples I and II due to the overlapping of the σ-relaxation. Moreover, the activation energies of the Goldstone mode, σ-, α-, and β-relaxations were decreased with increasing content of NLO dye. This is due to the plasticizer effect of the NLO dye. The plasticizer effect is not pronounced in the activation energies of the γ-relaxation. For sample III, the aggregation of the DO3 and the formation of the crystallites in the LC phase lead to the increase of the activation energy for all of the dielectric relaxations.

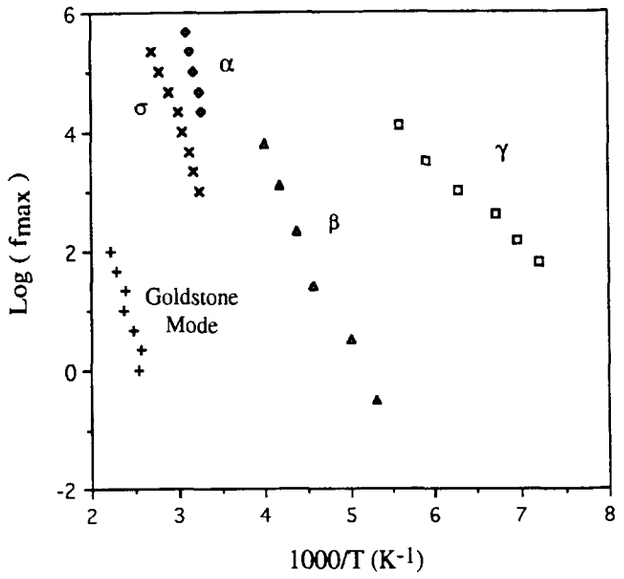

Figure 8 Temperature dependence of the relaxation frequencies for the γ, β, α, σ, and Goldstone mode relaxations of sample II

The Cole–Cole plots (ϵ'' vs ϵ') at different temperatures for the σ-relaxations of sample II are shown in *Figure 9*. In the Cole–Cole plot, the symbols represent the actual experiment data points and the curve is the arc of the best fitting circle. For the data close to the left-hand side of the circle, the appearance of the α-relaxation has been observed below 330 K, thereby causing the dielectric loss to increase at a higher frequency range (above 10^4 Hz) in the Cole–Cole plot for the σ-relaxation. The increase of the dielectric loss at this higher frequency range has been ignored for the curve fitting in the plots, because this is not part of the σ-relaxation. From the circle intersection with the ϵ' axis in the Cole–Cole plot, the dielectric relaxation intensity $[\Delta\epsilon'(T) = \epsilon'_0(T) - \epsilon'_\infty(T)]$ at different temperatures has been obtained. The σ-relaxation intensity as a function of temperature for samples I, II and III is given in *Figure 10*. The σ-relaxation intensity decreased with increasing temperature for samples I–III. This is because the high thermal energy results in a randomization in the orientation of the dipoles toward the alternating electric field with increasing temperature, and subsequently leads to the decrease of the relaxation intensity for the σ-relaxation[23]. Moreover, the σ-relaxation intensities of samples I and II were higher than that of sample III. Aggregation of the DO3

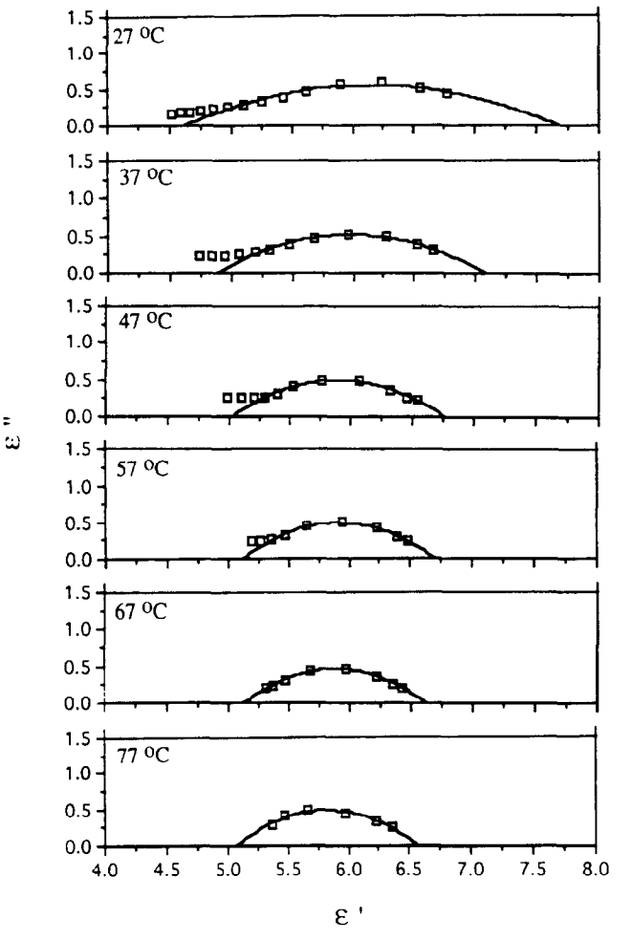

Figure 9 Cole–Cole plots of the σ-relaxation at different temperatures for sample II

molecules results in the decrease of the σ-relaxation intensity for sample III. In the case of samples I and II, the higher molecular mobility of the NLO dye in the LC phase was favourable for the electric poling process. In contrast, the lower molecular mobility of NLO dyes was observed for sample III. This will result in the decrease of the net noncentrosymmetry and SHG intensity of the material[24].

CONCLUSION

The molecular dynamics of the mixture of an NLO dye and an FLCP have been studied. The doping of the NLO dye in the LC phase leads to the increase of the

Table 2 Activation energies (kJ mol^{-1}) of the γ, β, α, σ and Goldstone mode relaxations for samples FLCP-III

Sample	Relaxation				Goldstone mode[b]
	γ[a]	β[b]	α[b]	σ[b]	
FLCP	34.0	76.0	418.0[c]–243.2[d]	—[e]	—[e]
I	31.0	73.2	227.7[c]	127.5[c]–65.7[d]	102.2
II	26.3	61.8	143.8[c]	115.7[c]–60.7[d]	93.5
III	36.1	65.4	200.0[c]–216.0[d]	128.7[c]–79.4[d]	107.2

[a] γ-relaxation ± 4 kJ mol^{-1}
[b] β, α, σ and Goldstone mode relaxations ± 15 kJ mol^{-1}
[c] The data were calculated at 10^3 Hz
[d] The data were calculated at 10^5 Hz
[e] The data could not be obtained

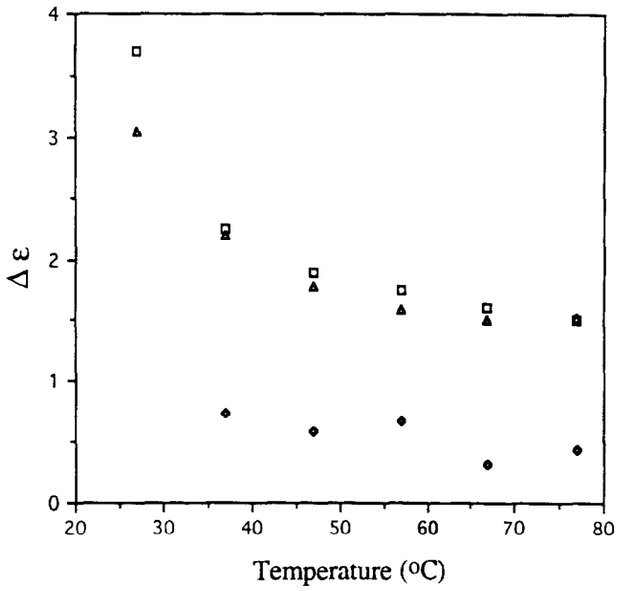

Figure 10 The relaxation intensity as a function of temperature for the σ-relaxation of samples I–III [I (□), II (△), and III (◇)]

thickness of the smectic layer in the S_C* phase. This results in the increase of the relaxation intensity and frequency of the Goldstone mode for the FLCP. Moreover, the activation energy of the Goldstone mode was decreased due to the plasticizer effect of the NLO dyes. As a result of that, the fluctuation of the spontaneous polarization vector in each smectic layer would be more active under an applied electric field. In addition, the NLO dye has high relaxation intensity in the LC phase for such guest–host material. The high relaxation intensity of the mesogenic group and NLO dye was favourable for the electric poling process. Furthermore, the relaxation intensity of the Goldstone mode and σ-relaxation was reduced when the excessive amount of the NLO dye was further added. The phase separation will lead to the reduction of the relaxation intensity for both the Goldstone mode of the FLCP and molecular mobility of the NLO dye. It is concluded that the doping of a suitable amount of the low molecular weight NLO dyes in the LC phase of the FLCP was helpful for the electric poling efficiency of such guest–host material.

ACKNOWLEDGEMENTS

The authors thank Prof. C. S. Hsu for providing FLCPs and the National Science Council of Republic of China for financial support of this work (Grant NSC84-2216-E007-029).

REFERENCES

1 Clark, N. A. and Lagerwall, S. T. *Appl. Phys. Lett.* 1980, **36**, 899
2 Beresnev, L. A. and Blinov, L. M. *Ferroelectrics* 1989, **92**, 335
3 Vtyurin, A. N., Yermakov, V. P., Ostrovsky, B. I. and Shabanov, V. F. *Krystallografiya* 1991, **26**, 546
4 Shtykov, N. M., Barnik, M. I., Beresnev, L. A. and Blinov, L. M. *Mol. Cryst. Liq. Cryst.* 1985, **124**, 379
5 Liu, J. Y., Robinson, M. G., Johnson, K. M., Wlaba, D. M., Ros, M. B., Clark, N. A., Shao, R. and Doroski, D. *J. Appl. Phys.* 1991, **70**, 3426
6 Schmitt, K., Herr, R. P., Schadt, M., Funfschilling, J., Buchecker, R., Chen, X. H. and Benecke, C. *Liq. Cryst.* 1993, **14**, 1735
7 Yoshino, K., Utsumi, M., Morita, Y., Sadohara, Y. and Ozaki, M. *Liq. Cryst.* 1993, **14**, 1021
8 Wischerhoff, E., Zentel, R., Redmond, M., Monval, O. M. and Coles, H. *Macromol. Chem. Phys.* 1994, **195**, 1593
9 Lee, R. H., Hsiue, G. H. and Jeng, R. J. 'Proc. IUPAC Int. Symp. on Functional and High Performance Polymers', Taipei, 1994, p. 611
10 Hsu, C. H., Shih, L. J. and Hsiue, G. H. *Macromolecules* 1993, **26**, 3161
11 Vallerien, S. U., Zentel, R., Kremer, F., Kapitza, H. and Fischer, E. W. *Makromol. Chem. Rap. Commun.* 1989, **10**, 333
12 Vallerien, S. U., Kremer, F., Kapitza, H., Zentel, R. and Fischer, E. W. *Ferroelectrics* 1990, **109**, 273
13 Vallerien, S. U., Kremer, F., Scherowsky, G., Schliwa, A., Kuhnpast, K. and Fischer, E. W. *Liq. Cryst.* 1990, **8**, 719
14 Kapitza, H., Zentel, R., Twieg, R. J., Nguyen, C., Vallerien, S. U., Kremer, F. and Wilson, C. G. *Adv. Mater.* 1990, **2**, 539
15 Vallerien, S. U., Kremer, F., Kapitza, H., Zentel, R. and Fischer, E. W. *Ferroelectrics* 1991, **113**, 231
16 Schonfeld, A., Kremer, F., Vallerien, S. U., Poths, H. and Zentel, R. *Ferroelectrics* 1991, **121**, 69
17 Hsiue, G. H., Lee, R. H., Jeng, R. J. and Chang, C. S. *J. Polym. Sci., Polym. Phys. Edn* 1996, **34**, 555
18 Kalmykov, Yu P. and Vij, J. K. *Liq. Cryst.* 1994, **17**, 741
19 Zentel, R. Strobl, G. R. and Ringsdorf, H. *Macromolecules* 1985, **18**, 960
20 Bristow, J. F. and Kalika, D. S. *Macromolecules* 1994, **27**, 1808
21 Malmstrom, E., Liu, F., Boyd, R. H., Hult, A. and Gedde, U. W. *Polym. Bull.* 1994, **32**, 679
22 Goodby, J. W. in 'Ferroelectric Liquid Crystals Principle, Properties and Application' (Ed. G. W. Taylor), Gordon and Breach Science Publishers, Philadelphia, 1991, Chap. 12, p. 207
23 Huo, P. and Cebe, P. *Macromolecules* 1992, **25**, 902
24 Hampsch, H. L., Yang, J., Wong, G. K. and Torkelson, J. M. *Macromolecules* 1990, **23**, 3640